



## Stilbene-benzophenone dyads for free radical initiating polymerization of methyl methacrylate under visible light irradiation



Xiaozhuan Qin<sup>a</sup>, Ge Ding<sup>a</sup>, Yulong Gong<sup>a</sup>, Chuan Jing<sup>a</sup>, Guangyue Peng<sup>a</sup>, Shihong Liu<sup>a</sup>, Lanying Niu<sup>a</sup>, Shengtao Zhang<sup>a,b</sup>, Ziping Luo<sup>a,b</sup>, Hongru Li<sup>a,b</sup>, Fang Gao<sup>a,b,\*</sup>

<sup>a</sup> College of Chemistry and Chemical Engineering, Chongqing University, Chongqing 400044, China

<sup>b</sup> National-municipal Joint Engineering Laboratory for Chemical Process Intensification and Reaction, Chongqing University, Chongqing 400044, China

### ARTICLE INFO

#### Article history:

Received 18 March 2016  
Received in revised form  
19 April 2016  
Accepted 22 April 2016  
Available online 27 April 2016

#### Keywords:

Photoinitiator  
Free radical  
Photopolymerization  
Electron transfer acrylate monomer

### ABSTRACT

The AB and AB<sub>2</sub> trans-stilbene-benzophenone dyads were synthesized through multi-step pathway. The target dyads showed remarkable absorption in visible light region. Visible light photoinitiating polymerization of methyl methacrylate by the new dyads was studied by photo-differential scanning calorimetry. The results suggested that the AB<sub>2</sub> dyad showed more efficient photoinitiating polymerization of methyl methacrylate than the AB one under visible light irradiation. Furthermore, the new dyads yielded the greater visible light photoinitiating polymerization effect than the intermolecular photoinitiating systems and the commercial photoinitiator titanocene respectively. The molecular weights of visible light photopolymers produced by the new dyads were determined by gel permeation chromatography. The visible light photoinitiating mechanism of the new dyads was analyzed by the static and transient absorption and emission spectra, electron spin resonance spectra and cyclic voltammograms. The thermal stabilities of the new dyads were further studied by differential scanning calorimetry and thermogravimetry.

© 2016 Elsevier Ltd. All rights reserved.

### 1. Introduction

In recent decades, the advances of long wavelength laser technologies have received considerable attentions since they have many superior advantages over short wavelength such as low energy and deep penetration [1,2]. Inspired by the development of long wavelength laser, the realization of highly efficient visible light photoinitiating polymerization systems becomes one of main concerns in medical and engineering fields such as dental clinical, coating, photoresist, printing plate, computer-to-plate, fabrication of microstructure, and so on [3–6].

So far, a few of approaches have been established to achieve the long wavelength photoinitiating polymerization [7–12]. For instance, Paczkowski and the coauthors proposed photo-induced intermolecular electron transfer to obtain long wavelength photoinitiating polymerization [7,8]. Normally, long wavelength organic dyes absorb visible light firstly, and then an intermolecular electron transfer process from dyes to ultraviolet photoinitiators occurs. It

leads to the yield of active free radicals for photoinitiating polymerization of monomers. Some squaraine dyes were demonstrated to efficiently photosensitize iodonium salts for the long wavelength photoinitiating polymerization of acrylate monomers [9,10].

It is obvious that this pathway is conveniently performed since there are many long wavelength photosensitizers and UV photoinitiators which can be employed to compose visible light photoinitiating polymerization systems. However, the further increase of long wavelength photoinitiating polymerization efficiencies of monomers becomes quite difficult since the production rates of active free radicals are limited by photoinduced intermolecular electron transfer.

It is well-accepted that photoinduced internal electron transfer is more rapid than the intermolecular electron transfer, and thus it can be used to get more efficient long wavelength photoinitiating polymerization. This suggests that the long wavelength photoinitiators play the significant roles in the achievement of efficient visible light photoinitiating polymerization [9,10]. While, the most of the photoinitiators such as 1,3,5-trichloromethyltriazine and benzophenone absorb very short ultraviolet light (200–300 nm), and they can not photoinitiate polymerization of monomers under visible light irradiation [13–15].

Therefore, it is necessary to prepare new long wavelength

\* Corresponding author. College of Chemistry and Chemical Engineering, Chongqing University, Chongqing 400044, China.

E-mail addresses: [stzhang@cqu.edu.cn](mailto:stzhang@cqu.edu.cn) (S. Zhang), [zpluo@126.com](mailto:zpluo@126.com) (Z. Luo), [hongruli1972@gmail.com](mailto:hongruli1972@gmail.com) (H. Li), [fanggao1971@gmail.com](mailto:fanggao1971@gmail.com) (F. Gao).

photoinitiators by molecular preporganization [16,17]. For instance, some efforts were successfully devoted to synthesize new cyanine dye-based photoinitiators for visible light photopolymerization of monomers [16–18]. While there are huge shortages of new long-wavelength photoinitiators in industrial applications due to the great challenges for rational molecular design of the target visible light photoinitiators.

It is well-known that the commercial long wavelength photoinitiator bis(cyclopentadienyl)-bis(2,6-difluoro-3-(1-pyrryl)-phenyl)titanium (titanocene) has the less absorption in visible light region ( $\epsilon_{\max}$  at 400 nm,  $\sim 10^3 \text{ cm}^{-1} \bullet \text{mol}^{-1} \bullet \text{L}$ ) and the weaker thermal stability (thermal decomposition  $< 300 \text{ }^\circ\text{C}$ ) since metal–C bond is not as strong as covalent chemical bond [19], and thus its application potentials are restrained. As a result, it is necessary to improve visible absorption strength and thermal stability of new visible light photoinitiators for the future application.

In this study, we propose that two or more UV photoinitiators are covalently attached to the same long-wavelength dye molecule for the development of new AB<sub>2</sub> or AB<sub>n</sub> dyads as the visible light photoinitiators. It is expected that the more efficient visible light photopolymerization can be achieved by the cooperative photoinduced intramolecular electron effect in AB<sub>2</sub> or AB<sub>n</sub> photoinitiators.

This work has established efficient synthesis approaches to develop the AB<sub>2</sub> trans-stilbene-benzophenone dyad. Meanwhile, the AB dyad was also prepared for the comparison of visible light photoinitiating efficiency. The intermolecular photoinitiating systems were also studied. We further compared the visible light photoinitiating effect of the new dyads to that of the commercial long wavelength photoinitiator titanocene. The visible light photoinitiating mechanism of the dyads was analyzed by the determinations of the static and transient absorption and emission spectra as well as ESR trapping spectra.

This study employed methyl methacrylate (MMA) as the representative acrylate monomer to evaluate visible light photoinitiation efficiencies of the new photoinitiators. The visible light photoinitiating polymerization of MMA by these new dyads was carried out by photo-differential scanning calorimetry. The results showed that AB<sub>2</sub> dyad photoinitiated polymerization of MMA more efficiently than the AB one under visible light irradiation. This study also demonstrated that the new dyads exhibited the greater visible light photoinitiating polymerization effect of MMA than the commercial long wavelength photoinitiator titanocene.

## 2. Experimental

### 2.1. Materials and structural characterization

The organic solvents were purchased from Aldrich Chemical Corporation and further dried using the standard laboratory methods [20]. The spectroscopically pure organic solvents employed in the spectral determination were provided by Aldrich as well. The coinitiator triethanolamine and the monomer MMA were also supplied by Aldrich. The chemical structures of the UV photoinitiators **C1**, **C2**, the dyads **C3** and **C4**, as well as the photosensitizer **C5** were shown in Fig. 1, which were prepared in our laboratory. **C1–C4** were firstly reported in this study. The chemical structures of these molecules were characterized by nuclear magnetic resonance (NMR) spectra, infrared spectra (IR) as well as elemental analysis.

Nuclear magnetic resonance apparatus (500 MHz) from Bruker were employed to determine <sup>1</sup>H and <sup>13</sup>C NMR spectra of the samples in the standard NMR tube by using tetramethylsilane (TMS) as an internal reference at room temperature. FT-IR spectra of the samples were detected by Fourier transform infrared spectrometer. A CE440 elemental analysis meter from Exeter Analytical Inc was

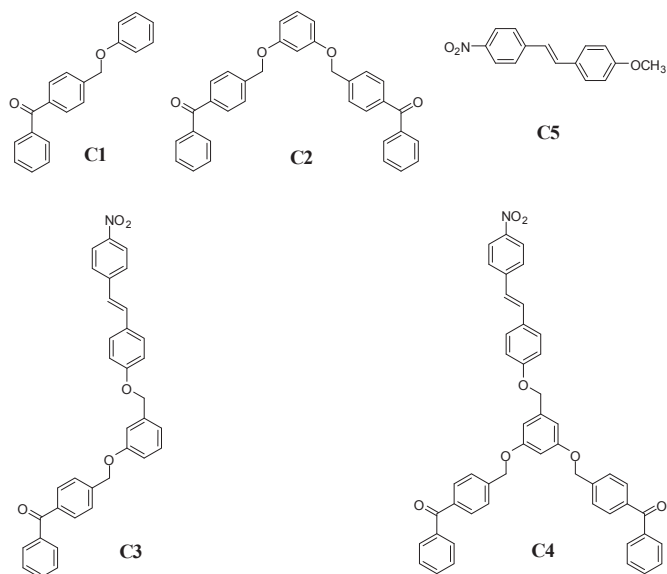


Fig. 1. Chemical structures of the studied molecules **C1–C5** in this work.

employed for the measurement of elemental analysis of the samples. The melting points of the samples were detected by a Beijing Fukai melting point apparatus. The UV/visible absorption spectra ( $1 \times 10^{-5} \text{ mol/L}$ ) of the samples were detected by a Cintra spectrophotometer. The fluorescence emission spectra of the samples were recorded by RF-531PC spectrofluorophotometer. The fluorescence quantum yields of the samples were measured by using quinine sulfate in 0.5 mol/L H<sub>2</sub>SO<sub>4</sub> ( $\Phi$ , 0.546) as the reference [21].

### 2.2. Visible light photoinitiating polymerization by photo-DSC study

Photo-differential scanning calorimetry (Photo-DSC) was carried out by Photo-DSC-204 F1 phoenix from Netzsch Corporation of Germany. A high pressure mercury lamp was utilized as the light source. Visible light was allowed to pass by cutting the UV wavelength light through the filter.

The organic formula was photoinitiated polymerization in open aluminum pans with a diameter of 6.6 mm. The empty aluminum pans were used as the blank. The experimental temperature was kept at 25 °C by a cooling system. The average power of visible light irradiation was 20 mW/cm<sup>2</sup> detected by a Coherent Model Field-master power meter (Germany).

Visible light photopolymerization kinetics of MMA was analyzed by the exothermal plots. The exothermic curves and the kinetics of free-radical photopolymerization reaction were monitored by measuring the heat flows during visible light irradiation. By integrating the area under the exothermic peak, the photopolymeric conversion of monomer MMA and the photopolymerization rate could be calculated from the reaction enthalpy flow according to the following equations:

$$C\% = \Delta H_t / \Delta H_0^{\text{theory}} \times 100\% \quad (1)$$

$$R_p = dC/dt = (dh/dt) / \Delta H_0^{\text{theory}} \quad (2)$$

Where in C% was double bond polymerization conversion,  $\Delta H_t$  showed the reaction heat evolved at irradiation time  $t$  and  $\Delta H_0^{\text{theory}}$  represented the theoretical heat of the complete conversion. For the double bond of MMA,  $\Delta H_0^{\text{theory}}$  was 86 kJ/mol [22].  $R_p$  meant the photopolymerization rate and  $dh/dt$  was the reaction enthalpy flow

measured by the DSC curve.

### 2.3. Gel permeation chromatography (GPC) analysis

Number average molecular weight ( $M_n$ ) and weight average molecular weight ( $M_w$ ) of photopolymer PMMA yielded by the studied visible light photoinitiating systems in organic solvents were determined by gel permeation chromatography (GPC). Variations of molecular weights and polydispersity index (PDI) of polymethyl methacrylate (PMMA) were monitored by a Shimadzu GPC instrument with tetrahydrofuran (HPLC grade, Sigma–Aldrich Co, USA) as the mobile phase at a low rate of 1 mL/min and oven temperature of 40 °C. Polystyrene standards with the narrow molecular weight distributions were used for the calibration.

### 2.4. Laser flash photolysis

The samples were thoroughly deaerated by bubbling with Ar for 1 h before the measurement in the dark room. The experiments were conducted in a rectangular quartz cell with a path length of 5 mm along the monitoring light path. Nanosecond laser flash photolysis of the samples was performed by a 355 nm laser pulse. A 300 W xenon lamp was used as the monitoring source. The transmitted monitoring light from the sample was collected and focused onto a monochromator, and the signals were processed by a computer system.

### 2.5. Electron spin resonance (ESR) analysis

The electron spin resonance (ESR) spectra of samples was performed by Bruker EMX EPR spectrometer at 9.5 GHz with a modulation frequency of 200 kHz. 5,5-Dimethyl-pyrroline-N-oxide (DMPO) was utilized as the radical capturing agent. The new dyad and coinitiator were dissolved in ethyl acetate ( $2 \times 10^{-4}$  mol/L), and then 0.5 mL solution was placed into a quartz ESR tube and then purged with  $N_2$  for half an hour to remove oxygen.

### 2.6. Cyclic voltammograms determination

Cyclic voltammograms was determined in a Shanghai Chenhua working station. A representative three-electrode system including two platinum work electrodes and an Ag/AgCl reference electrode were used in the cell. A 0.05 mol/L solution of tetra-n-butylammonium hexafluorophosphate in dichloromethane containing the samples was bubbled with Ar for 30 min before the measurement.

### 2.7. Thermal stable analysis

The differential scanning calorimetry (DSC) and thermogravimetry (TG) analysis of the samples were conducted under  $N_2$  flow at 100 mL/min in Shimadzu-DTG-60H at a heating rate 20 °C/min, and the temperature range was 0–600 °C.

### 2.8. Preparation of the new target dyads

The new dyads (**C3** and **C4**) were prepared through multi-step approaches shown in [Scheme 1](#). The synthesis of the other target molecules **C1**, **C2** and **C5** were also provided in [Scheme 1](#).

#### 2.8.1. Synthesis of 4-bromomethyl-benzophenone

The title molecule was synthesized according to the previous report [\[23\]](#).

#### 2.8.2. Synthesis of 4-nitrostyryl-phenol and **C5** (4-nitro-4'-methoxyl-styrene)

The titled two compounds were prepared according to the previous literature [\[24\]](#).

#### 2.8.3. Synthesis of 4-phenoxy-methyl-benzophenone (**C1**)

In a three-necked flask, 4-bromomethyl-benzophenone 0.5 g (2.9 mmol) and phenol 0.4 g (4.3 mmol) were added into 20 mL dry acetone including potash 0.8 g (5.8 mmol) and a little 18-Crown-6. The mixture was stirred at room temperature overnight under Ar atmosphere. After the reaction, the solid of potassium carbonate was filtrated and acetone was evaporated in a vacuum system. And then, the reactant mixture was dissolved in chloroform and washed by water, and the organic layer was dried by anhydrous sodium sulfate. The product was purified with column chromatography by using benzene as the eluent, which was further recrystallized in *n*-hexane. Color: white; yield: 82.4%; m.p: 141.2–142.5 °C;  $^1H$  NMR ( $D^6$ -DMSO, 500 MHz)  $\delta$ (ppm): 7.746–7.706 (m, 4H, Ar–H), 7.665–7.641 (t, 1H, Ar–H), 7.610–7.596 (d, 2H, J = 7.0 Hz, Ar–H), 7.550–7.524 (t, 2H, Ar–H), 7.295–7.269 (t, 2H, Ar–H), 7.019–7.005 (d, 2H, J = 7.0 Hz, Ar–H), 6.943–6.919 (t, 1H, Ar–H), 5.282 (s, 2H, Ar–CH<sub>2</sub>–);  $^{13}C$  NMR ( $D^6$ -DMSO, 125 MHz)  $\delta$ (ppm): (194.506, 159.002, 140.514, 138.444, 137.493, 132.421, 130.600, 130.513, 130.413, 130.312, 129.812, 129.717, 129.212, 129.115, 128.399, 128.319, 121.009, 114.712, 114.671, 70.789); Anal. Calcd for  $C_{20}H_{16}O_2$  (288.12): C, 83.31, H, 5.59, Found: C, 83.42, H, 5.51.

#### 2.8.4. Synthesis of 1, 3-bis(4-benzoyl)benzyloxy)-benzene (**C2**)

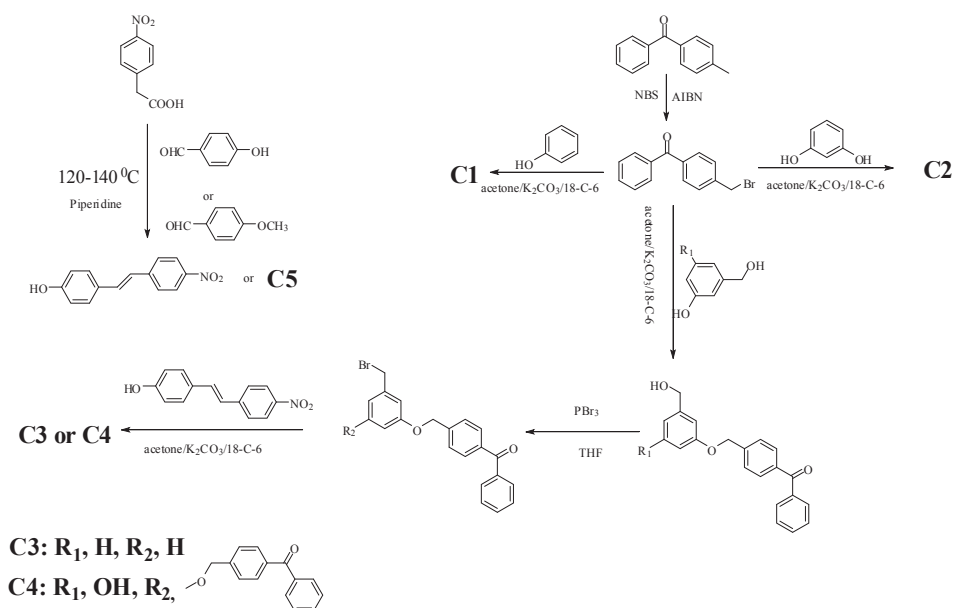
The synthetic method of **C2** was the same as that of **C1**, using benzene-1,3-diol to replace phenol. Color: white; yield: 81.5%; m.p: 154–155.3 °C;  $^1H$  NMR ( $D^6$ -DMSO, 500 MHz)  $\delta$ (ppm): 7.742–7.699 (m, 8H, Ar–H), 7.661–7.637 (t, 2H, Ar–H), 7.597–7.584 (d, 4H, J = 6.5 Hz, Ar–H), 7.543–7.519 (t, 4H, Ar–H), 7.208–7.181 (t, 1H, Ar–H), 6.712 (s, 1H, Ar–H), 6.638–6.621 (m, 2H, Ar–H), 5.197 (s, 4H, Ar–CH<sub>2</sub>–);  $^{13}C$  NMR ( $D^6$ -DMSO, 125 MHz)  $\delta$ (ppm): (194.311, 194.305, 161.613, 161.554, 140.445, 140.413, 138.394, 138.374, 137.313, 137.301, 132.415, 132.299, 130.712, 130.613, 130.567, 130.488, 130.313, 130.301, 130.297, 130.273, 129.112, 129.105, 129.101, 129.094, 129.004, 128.412, 128.394, 128.374, 128.335, 106.623, 106.545, 100.394, 70.821, 70.724); Anal. Calcd for  $C_{34}H_{26}O_4$  (498.18): C, 81.91, H, 5.26, Found C, 82.04, H, 5.17.

#### 2.8.5. Synthesis of 1-(4-(4-benzoyl)-benzyloxy)-phenemethylol

The synthetic method of the titled molecule was similar to that of **C1** and **C2**. 3-Hydroxymethyl-phenol 1.0 g (8.1 mmol) and 1,3-bis(4-benzoyl)benzyloxy)benzene 2.9 g (10.4 mmol) were used as the starting materials. Color: yellow; yield: 75.7%; m.p: 131.2–132.8 °C;  $^1H$  NMR ( $D^6$ -DMSO, 500 MHz)  $\delta$ (ppm): 7.778–7.718 (t, 4H, Ar–H), 7.644–7.555 (m, 3H, Ar–H), 7.461 (s, 2H, Ar–H), 7.275–7.248 (d, 2H, J = 13.5 Hz, Ar–H), 7.033–6.927 (m, 2H, Ar–H), 5.271 (s, 1H, –OH), 5.161 (s, 2H, Ar–CH<sub>2</sub>–), 4.610 (s, 2H, Ar–CH<sub>2</sub>–);  $^{13}C$  NMR ( $D^6$ -DMSO, 125 MHz)  $\delta$ (ppm): (194.311, 157.911, 140.413, 138.411, 137.321, 133.515, 132.411, 130.582, 130.552, 130.311, 130.303, 129.325, 129.311, 129.111, 129.101, 128.411, 128.401, 114.511, 114.507, 70.811, 64.703). Anal. Calcd for  $C_{21}H_{18}O_3$  (318.13): C, 79.22, H, 5.70, Found: C 79.13, H, 5.62.

#### 2.8.6. Synthesis of 1-(4-(4-benzoyl)-benzyloxy)-bromomethyl-benzene

Phosphorus tribromide 1.3 g (4.9 mmol) and 1-(4-(4-benzoyl)benzyloxy)phenemethylol 1.4 g (3.8 mmol) were added into 40 mL dry tetrahydrofuran in a three-necked flask. The reaction was protected by argon atmosphere and stirred at room temperature for 5 h. The solvent was evaporated in vacuum and the crude product was dissolved in chloroform, then washed by sodium bicarbonate



**Scheme 1.** The multi-step synthesis approach of new dyads.

solution and extracted by dichloromethane. The organic layer was dried by anhydrous sodium sulfate. The product was purified through column chromatography by using the mixed solvent (cyclohexane/dichloromethane = 1/4, v/v) as the eluent. The light yellow product was obtained. Yield: 64.6%; m.p.: 127–128.5 °C; <sup>1</sup>H NMR (D<sup>6</sup>-DMSO, 500 MHz) δ(ppm): 7.745–7.713 (m, 4H, Ar–H), 7.643–7.558 (t, 3H, Ar–H), 7.432–7.415 (d, 2H, J = 8.5 Hz, Ar–H), 7.013–6.945 (m, 4H, Ar–H), 5.083 (s, 2H, Ar–CH<sub>2</sub>–O–), 4.432 (s, 2H, Ar–CH<sub>2</sub>–Br–); <sup>13</sup>C NMR (D<sup>6</sup>-DMSO, 125 MHz) δ(ppm): (194.301, 159.211, 140.423, 138.411, 137.293, 132.294, 130.285, 130.265, 130.243, 130.231, 130.223, 130.110, 130.105, 129.189, 129.101, 128.414, 128.401, 114.611, 114.607, 70.818, 33.321); Anal. Calcd for C<sub>21</sub>H<sub>17</sub>BrO<sub>2</sub>: C, 66.16, H, 4.49, Found: C 66.25, H, 4.40.

#### 2.8.7. Synthesis of 3,5-bis((4-benzoyl)benzyloxy)phenylcarbinol

4-Bromomethyl-benzophenone 0.685 g (2.5 mmol) and 5-hydroxymethyl-benzene-1,3-diol 0.14 g (1.0 mmol) were mixed in a flask. Dry acetone (30 mL) containing potash 0.69 g (5.0 mmol) and a little 18-Crown-6 was gradually added. The mixture was stirred at room temperature overnight under Ar atmosphere. After the reaction, the purification of the product was similar to that of **C1**. Color: yellow; yield: 69.4%; m.p.: 131–132 °C; <sup>1</sup>H NMR (D<sup>6</sup>-DMSO, 125 MHz) δ(ppm): 7.779–7.732 (m, 8H, Ar–H), 7.698–7.688 (t, 2H, J = 7.5 Hz, Ar–H), 7.633–7.616 (d, 4H, J = 8.5 Hz, Ar–H), 7.581–7.551 (t, 4H, Ar–H), 6.661–6.612 (d, 3H, J = 24.5 Hz, Ar–H), 5.247–5.240 (s, 1H, –OH), 5.240–5.225 (s, 4H, –CH<sub>2</sub>–O–), 4.467–4.464 (s, 2H, –CH<sub>2</sub>–); <sup>13</sup>C NMR (D<sup>6</sup>-DMSO, 125 MHz) δ(ppm): (194.113, 194.003, 159.911, 159.857, 143.211, 140.409, 140.384, 138.356, 138.314, 137.312, 137.002, 132.411, 132.411, 130.511, 130.501, 130.312, 130.301, 130.299, 130.274, 130.253, 130.223, 129.112, 129.089, 129.071, 129.021, 128.421, 128.411, 128.394, 128.341, 105.817, 105.065, 98.311, 70.547, 70.318, 65.286); Anal. Calcd for C<sub>35</sub>H<sub>28</sub>O<sub>5</sub> (528.19): C, 79.53, H, 5.34, Found: C, 79.61, H, 5.25.

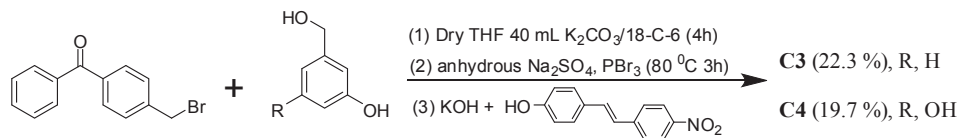
#### 2.8.8. Synthesis of 3,5-bis((4-benzoyl)-benzyloxy)-benzyl bromide

Phosphorus tribromide 1.3 g (4.9 mmol) and 3,5-bis((4-benzoyl)-benzyloxy)-phenylcarbinol 2 g (3.8 mmol) were added into 40 mL dry tetrahydrofuran in a three-necked flask. The

reactant was protected by argon atmosphere and stirred at room temperature for 5 h. The solvent was evaporated in vacuum and the crude product was dissolved in chloroform, then washed by sodium bicarbonate solution and extracted by dichloromethane. The organic layer was dried by anhydrous sodium sulfate. After the solvent was removed, the product was further purified with column chromatography by using the mixed solvents (cyclohexane/dichloromethane, 1/4, v/v) as the eluent. Color: yellow; yield: 66.3%; m.p.: 134.2–135.4 °C; <sup>1</sup>H NMR (D<sup>6</sup>-DMSO, 500 MHz) δ(ppm): 7.814–7.797 (m, 8H, Ar–H), 7.614–7.584 (t, 2H, Ar–H), 7.551–7.527 (d, 4H, J = 12.0 Hz, Ar–H), 7.504–7.474 (t, 4H, Ar–H), 6.676–6.567 (d, 3H, J = 15.5 Hz, Ar–H), 5.141–5.092 (s, 4H, –CH<sub>2</sub>–O–), 4.430 (s, 2H, –CH<sub>2</sub>–); <sup>13</sup>C NMR (D<sup>6</sup>-DMSO, 125 MHz) δ(ppm): (194.127, 194.006, 160.503, 160.019, 140.463, 140.193, 140.082, 138.375, 138.164, 137.329, 137.281, 132.441, 132.192, 130.619, 130.459, 130.413, 130.327, 130.293, 130.247, 130.182, 130.131, 129.316, 129.204, 129.114, 129.009, 128.473, 128.358, 128.273, 128.117, 106.821, 106.759, 100.036, 70.886, 70.349, 33.149); Anal. Calcd for C<sub>35</sub>H<sub>27</sub>BrO<sub>4</sub>: C 71.07, H, 4.60, Found: C, 71.17, H, 4.53.

#### 2.8.9. Synthesis of 1-(4-(4-nitro-styryl)-phenoxy)methylene)-3-((4-benzoyl)benzyloxy)-benzene (**C3**)

1-(4-(4-Benzoyl)-benzyloxy)-bromomethyl-benzene 1 g (2.6 mmol) reacted with 4-nitro-styryl-phenol 0.948 g (3.9 mmol) in dry acetone including potash 0.72 g (5.2 mmol) and a little 18-Crown-6 under argon atmosphere at room temperature overnight. After the reaction, the solid was filtrated, and the solvent was evaporated by a vacuum system. After then, the reactant mixture was dissolved in chloroform and washed by water. The organic layer was dried by anhydrous sodium sulfate. After the solvent was removed, **C3** was purified with column chromatography by using the mixed solvents as the eluent (cyclohexane/dichloromethane, 3/1, v/v). The product was further purified with recrystallization in dichloromethane. **C3**: color: yellow; yield: 56.5%; m.p.: 183.0–184.5 °C; <sup>1</sup>H NMR (D<sup>6</sup>-DMSO, 500 MHz) δ(ppm): 8.194–8.179 (d, 2H, J = 7.5 Hz, Ar–H), 7.789–7.774 (d, 2H, J = 7.5 Hz, Ar–H), 7.747–7.705 (m, 4H, Ar–H), 7.666–7.641 (t, 1H, J = 6.5 Hz, Ar–H), 7.615–7.583 (m, 4H, Ar–H), 7.550–7.524 (m, 2H, Ar–H), 7.460–7.432 (d, 1H, J = 14.0 Hz, Ar–CH=CH–), 7.320–7.294 (t, 1H,



**Scheme 2.** The one-pot preparation method of new photoinitiators **C3** and **C4**.

$J = 6.5$  Hz, Ar–H), 7.248–7.221 (d, 1H,  $J = 13.5$  Hz, Ar–CH=CH–), 7.121 (s, 1H, Ar–H), 7.039–6.975 (m, 4H, Ar–H), 5.228 (s, 2H, –CH<sub>2</sub>–O–), 5.111 (s, 2H, –CH<sub>2</sub>–O–); <sup>13</sup>C NMR (D<sup>6</sup>-DMSO, 125 MHz)  $\delta$ (ppm): (195.918, 159.302, 158.740, 146.282, 144.960, 142.470, 139.088, 137.493, 136.835, 133.449, 133.179, 130.360, 130.163, 130.086, 129.636, 129.101, 129.066, 128.798, 127.860, 127.370, 124.620, 124.519, 120.687, 115.686, 114.639, 114.581, 69.555, 69.043). IR (cm<sup>-1</sup>): 3129.6, 3035.5, 1649.9, 1586.7, 1508.5, 1400.5, 1340.9, 1306.6, 1256.4, 1174.4, 1154.7, 1109.5, 1047.9, 1021.1, 941.5, 844.5, 737.3, 705.8. Anal. Calcd for C<sub>35</sub>H<sub>27</sub>NO<sub>5</sub> (541.19): C, 77.62, H, 5.02, N, 2.59, Found: C, 77.71, H, 4.91, N, 2.67.

### 2.8.10. Synthesis of 1-(4-(4-nitrostyrene)-phenoxy)methylene)-3,5-bis((4-benzoyl)benzyloxy)-benzene (**C4**)

The reaction of 3,5-bis((4-benzoyl)benzyloxy)benzyl bromide 1 g (1.7 mmol) and 4-nitrostyryl-phenol 0.61 g (2.5 mmol) was mixed in acetone including potassium carbonate 0.468 g (3.3 mmol) and a little 18-Crown-6 under Ar atmosphere at room temperature overnight. The purification of **C4** was carried out as that of **C3**, color: yellow; yield: 52.1%; m.p: 142.8–144.5 °C; <sup>1</sup>H NMR (D<sup>6</sup>-DMSO, 500 MHz)  $\delta$ (ppm): 8.190–8.176 (d, 2H,  $J = 7.0$  Hz, Ar–H), 7.777–7.762 (d, 2H,  $J = 7.5$  Hz, Ar–H), 7.742–7.728 (d, 4H,  $J = 7.0$  Hz, Ar–H), 7.710–7.679 (d, 4H,  $J = 15.5$  Hz, Ar–H), 7.662–7.637 (t, 2H,  $J = 6.5$  Hz, Ar–H), 7.600–7.571 (m, 6H, Ar–H), 7.544–7.518 (m, 4H,  $J = 13.0$  Hz, Ar–H), 7.444–7.416 (d, 1H,  $J = 14.0$  Hz, Ar–CH=CH–), 7.235–7.207 (d, 1H,  $J = 14.0$  Hz, Ar–CH=CH–), 7.023–7.009 (d, 2H,  $J = 7.0$  Hz, Ar–H), 5.216 (s, 4H, –CH<sub>2</sub>–O–), 5.080 (s, 2H, –CH<sub>2</sub>–O–); <sup>13</sup>C NMR (D<sup>6</sup>-DMSO, 125 MHz)  $\delta$ (ppm): (195.399, 159.405, 158.787, 145.815, 144.469, 141.839, 139.574, 136.985, 136.355, 132.925, 132.670, 129.855, 129.559, 129.157, 128.589, 128.551, 128.313, 127.959, 127.774, 127.58, 127.370, 126.864, 124.132, 124.006, 115.202, 106.690, 101.264, 69.029, 69.207). IR (cm<sup>-1</sup>): 3430.6, 3128.0, 3032.7, 1655.5, 1596.2, 1508.9, 1448.2, 1407.2, 1337.4, 1318.6, 1277.9, 1248.2, 1163.2, 1145.9, 1109.1, 1047.8, 824.7, 788.3, 705.9; Anal. Calcd for C<sub>49</sub>H<sub>37</sub>NO<sub>7</sub> (751.26): C, 78.28, H, 4.96, N, 1.86, Found: C, 78.37, H 4.87, N 1.94.

## 3. Results and discussion

### 3.1. Synthesis and <sup>1</sup>H NMR characterization of the new target dyads

The multi-step synthesis strategy has been established to prepare the new dyads **C3** and **C4**. The reaction was mainly involved with bromination of hydroxy group as well as the following condensation reaction between phenolic hydroxy and benzyl bromide derivatives. Fortunately, the purified yields of **C3** and **C4** were reasonable in both the last steps and the total routes (such as **C4**, the last step, 52.1%, the total route, 24.0%).

In order to simplified the preparation route, one-pot synthesis of **C3** and **C4** was made based on the optimized experimental conditions. Scheme 2 showed one-pot preparation process developed in our lab, which provide the similar yields of **C3** and **C4** as the multi-step synthesis method.

Fig. 2 gave the representative <sup>1</sup>H NMR spectra of the target dyads **C3** and **C4**. The results demonstrated that benzophenone was attached to the dye molecular scaffold through chemical covalent

bond. It was noticed that the –OCH<sub>2</sub>– segments in **C3** or **C4** obviously displayed two separated peaks, reflecting that they are located in different chemical environments. The <sup>1</sup>H NMR spectral integration area ratio of different hydrogen atoms was consistent with that of the numbers of hydrogen atoms. We also found that carbonyl group led to the movement of <sup>1</sup>H NMR peaks of its adjacent hydrogen atoms to the down magnetic field due to its electron withdrawing effect. Furthermore, the stronger electron accepting role of nitro group caused the greater shift <sup>1</sup>H NMR peaks of its adjacent hydrogen atoms to the lower magnetic field.

Therefore, the successful synthesis of the target photoinitiators means the possibility of the large scale preparation of the new dyads **C3** and **C4**, which affords the great potentials for the further applications.

### 3.2. UV/visible absorption properties of the new dyads

The UV/visible absorption spectra of **C1**–**C5** were determined in various organic solvents. The typical absorption spectra of these molecules in ethyl acetate were presented in Fig. 3. The results showed that **C3** and **C4** yielded the remarkable absorption in the above 400 nm region. We need to point out that the molar extinction coefficients of **C3** and **C4** at around 400 nm are two orders of magnitude larger than that of the commercial photoinitiator titanocene (~10<sup>5</sup> cm<sup>-1</sup> M<sup>-1</sup>, versus ~10<sup>3</sup> cm<sup>-1</sup> M<sup>-1</sup> [19]). The representative absorption parameters of these molecules in various solvents were given Table 1.

Fig. 1 showed that **C1** and **C2** possessed the single absorption band peaked at near 260 nm, which was generated by benzophenone part. While in contrast, **C3** and **C4** displayed the double absorption bands, which included the first absorption band peaked at about 260 nm yielded by benzophenone part, and the second absorption band peaked at approximate 370 nm produced by chromophore part.

**C4** exhibited the similar maximal molar extinction coefficients at around 260 nm as **C2** in various solvents. The maximal molar extinction coefficients of **C2** and **C4** at about 260 nm were approximate two times as large as those of **C1** and **C3** (such as in EtOAc, **C4**, 0.395 at 256 nm, **C3**, 0.198 at 256 nm, **C2**, 0.383 at 258 nm, **C1**, 0.188 at 256 nm). This further demonstrated that benzophenone part was covalently attached to the dye molecular backbone. The presence of two benzophenone parts in **C2** and **C4** produced nearly twice molar extinction coefficients at near 260 nm comparing to **C1** and **C3**.

On the other hand, to **C3** and **C4**, the maximal absorption wavelengths and the maximal molar extinction coefficients of the second absorption band peaked at around 370 nm were close with each other (such as in EtOAc, **C4**, 0.198 at 373 nm, **C3**, 0.179 at 374 nm, **C5**, 0.200 at 377 nm). This is mainly due to the presence of single chromophore part in **C3** and **C4**. As a consequence, **C5** produced the similar absorption spectral properties as **C3** and **C4** in the long wavelength region in various solvents. It was observed that the maximal absorption wavelength of **C3** and **C4** shifted to the longer wavelength in polar solvents (such as to **C4**, in 1,4-dioxane, 360 nm, in ACN, 371 nm), which could be caused by the presence of intramolecular charge transfer in the ground state of the entire



**Table 1**

The UV spectral parameters of **C1–C4** in various solvents,  $\lambda_{a,max}$ , the absorption maximum (nm),  $\epsilon_{max}$ , the maximal molar extinction coefficient ( $\text{cm}^{-1}\cdot\text{mol}^{-1}\cdot\text{L}$ ,  $\times 10^5$ ).

Photoinitiators	Solvents									
	1,4-Dioxane		Ethyl acetate		THF		CH <sub>2</sub> Cl <sub>2</sub>		CH <sub>3</sub> CN	
	$\lambda_{max}$	$\epsilon$	$\lambda_{max}$	$\epsilon$	$\lambda_{max}$	$\epsilon$	$\lambda_{max}$	$\epsilon$	$\lambda_{max}$	$\epsilon$
<b>C1</b>	255	0.183	258	0.188	263	0.197	256	0.224	255	0.208
<b>C2</b>	255	0.374	258	0.383	261	0.376	256	0.418	257	0.376
<b>C3</b>	363	0.125	374	0.179	370	0.120	367	0.161	369	0.206
<b>C4</b>	360	0.131	373	0.198	372	0.133	378	0.159	371	0.239

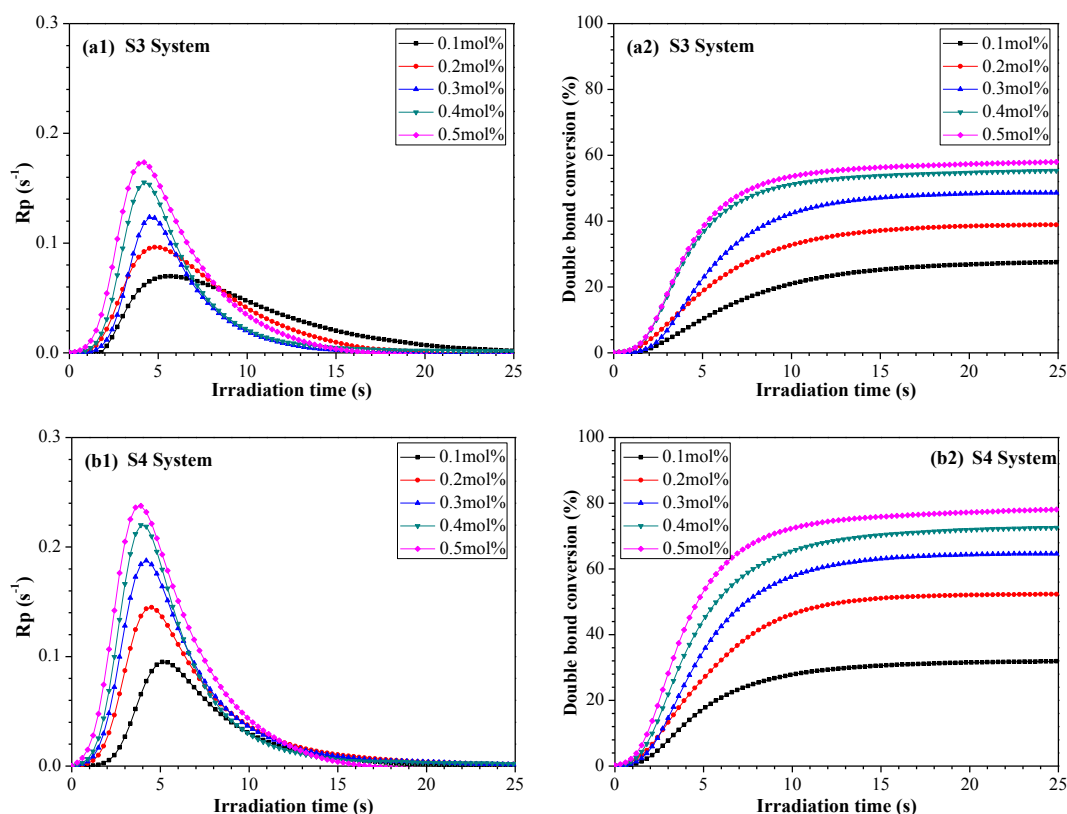


**Fig. 4.** (Left/a1, b1) The kinetic curves of visible light photopolymerization of MMA photoinitiated by **S3** and **S4** systems respectively at room temperature. (Right/b1, b2) The relationship between the photopolymerization conversion percent of double bond of ( $-\text{CH}=\text{CH}-$ ) of MMA and the irradiation time. The concentrations of photoinitiators, **C3** or **C4** and the cointiator (line— $\blacksquare$ — 0.1 mol%, line— $\bullet$ — 0.2 mol%, line— $\blacktriangle$ — 0.3 mol%, line— $\blacktriangledown$ — 0.4 mol%, line— $\blacklozenge$ — 0.5 mol%). Irradiation intensity,  $I_a$ , 20 mW/cm<sup>2</sup>.

photoinitiator **C1** or **C2** and triethanolamine) under visible light irradiation due to the absence of the long wavelength absorption ( $>400$  nm).

The new dyads **C3** and **C4** were found to display the favorable solubility in organic formulation. The relationship between the visible light photoinitiating polymerization efficiencies of MMA and the concentrations of the photoinitiators or the irradiation time

were studied by photo-DSC. The representative plots of the photoinitiating polymerization rates of MMA and the conversions of double bond of MMA at various concentrations of the photoinitiators with visible light irradiation time were shown in Fig. 4. The results suggested that the photoinitiating system **S4** reached the maximal photoinitiating polymerization rate in a shorter irradiation time than the photoinitiating system **S3** at the same

**Table 2**

The visible light photoinitiated polymerization kinetics parameters at different concentrations of **C3** or **C4**, Photopolymerization rate  $R_{p,max}$  ( $\text{s}^{-1}$ ), Double bond polymerization conversion C% (%).

Concentrations of the photoinitiators (mol%)	<b>C3</b>			<b>C4</b>		
	$R_{p,max}$ ( $\text{s}^{-1}$ )	Conversion (%)	$T_{max}$ (s)	$R_{p,max}$ ( $\text{s}^{-1}$ )	Conversion (%)	$T_{max}$ (s)
0.1	0.069	26.5	5.5	0.095	30.8	5.1
0.2	0.096	38.1	5.0	0.145	51.6	4.4
0.3	0.122	48.1	4.7	0.188	63.7	4.1
0.4	0.153	54.6	4.2	0.218	71.5	3.9
0.5	0.174	57.5	4.0	0.237	76.9	3.7

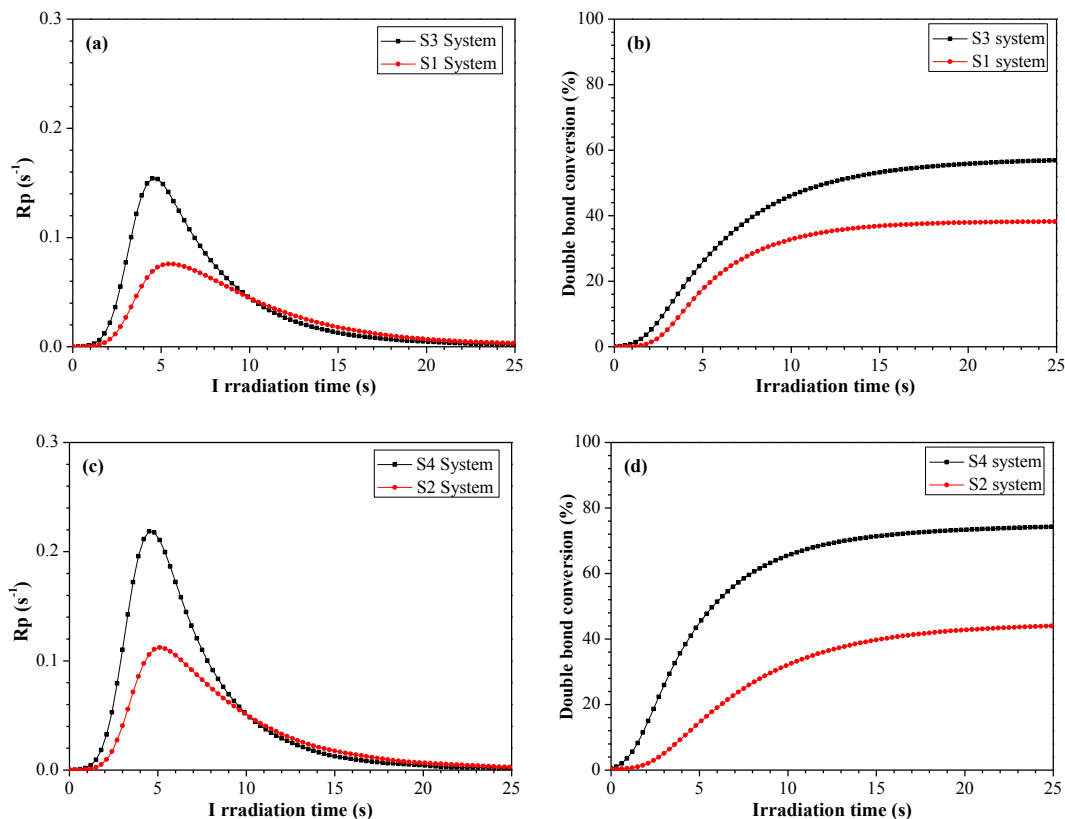


**Fig. 5.** (Left/(a), (c)) The kinetic curves of visible light photopolymerization of MMA photoinitiated by **S3** system (**C3**, triethanolamine) and **S1** system (**C1**, **C5** and triethanolamine), **S4** system (**C4**, triethanolamine) and **S2** system (**C2**, **C5** and triethanolamine) at room temperature. (Right/(b),(d)) The relationship between the photopolymerization conversion percent of double bond ( $-\text{CH}=\text{CH}-$ ) of MMA and visible light irradiation time. The concentrations of the photoinitiators, the photosensitizers and the coinitiator were 0.4 mol% respectively. Irradiation intensity, 20 mW/cm<sup>2</sup>

conditions. This reflected that **C4** could more efficiently produce active free radicals than **C3** under visible light irradiation.

It was also observed that as soon as the photoinitiating polymerization rates of **S3** and **S4** systems reached the peak values, a gradual decrease was observed with the extension of visible light irradiation time at the different concentrations of the photoinitiators. The results could be ascribed to the following factors: (1)

the photoinitiating polymerization materials were largely consumed [26], (2) the yielded photopolymers increased the viscosity of the systems, and the photoinitiating polymerization reaction could be inhibited accordingly, (3) the coupling rate of free radicals increased as more radicals were yielded.

Fig. 4 also suggested that the photoinitiating polymerization rates of **S3** and **S4** systems exhibited the increase with the increase of the concentrations of the photoinitiators. On the other hand, the

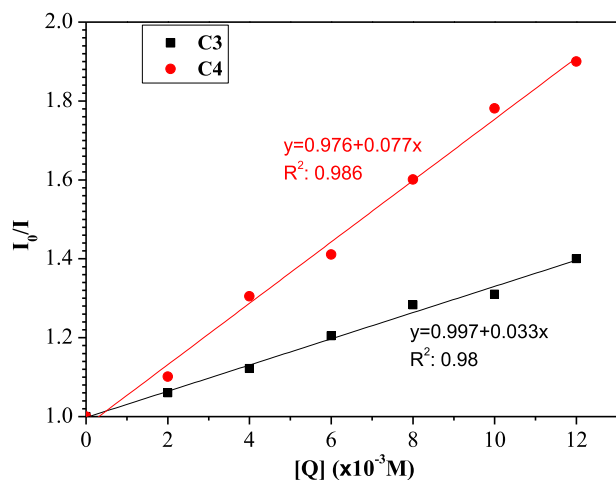


**Fig. 6.** Stern–Volmer plots of the dyads by the quencher triethanolamine (Q) in ethyl acetate,  $I_0$ , fluorescence intensity of the dyads,  $I$ , fluorescence intensity in the presence of the quencher, the concentration of the dyads:  $1.0 \times 10^{-5}$  mol L<sup>-1</sup>, excited at 350 nm.

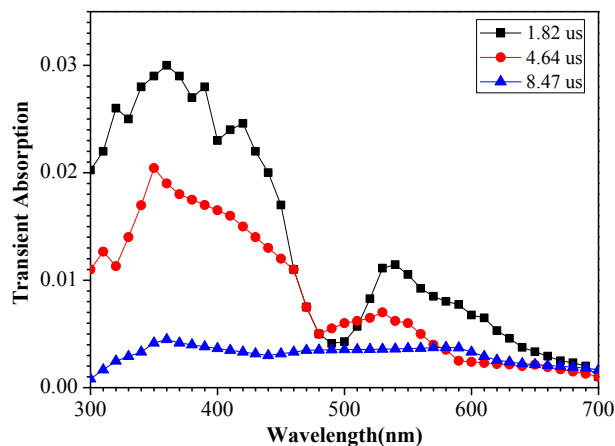


**Fig. 7.** The transient absorption spectra recorded 1.82  $\mu\text{s}$ , 4.64  $\mu\text{s}$  and 8.47  $\mu\text{s}$  following laser excitation (355 nm) of the dyads in Ar saturated ethyl acetate solution at room temperature, the concentration of the dyads,  $3.0 \times 10^{-5}$  mol L<sup>-1</sup>

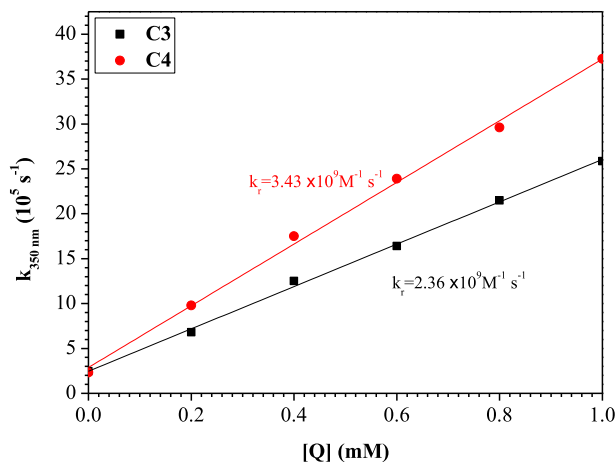


**Fig. 8.** The reaction of the quencher triethanolamine (Q) with the triplet dyes at room temperature. Dependence of the pseudo-first-order rate constant of the decay of the optical absorption at 350 nm on the concentration of the quencher after laser excitation (355 nm).

photoinitiating polymerization rates of **S3** or **S4** systems tended to slightly increase as the concentrations of the photoinitiator **C3** or **C4** reached certain critical values. Hence, the double bond conversions of MMA in **S3** or **S4** systems increased with the increase of the concentrations of photoinitiators **C3** or **C4** firstly, while they tended to be stable as the concentrations of the photoinitiator reached some values at the same irradiation time (**Figures 4b1** & **4b2**). The excess radicals could be yielded at the higher concentrations of the photoinitiators, which could increase the radical coupling effect as well as some side effects like radical chain-transfer reaction or superabundant radicals acting as the impurities and polymerization inhibitor. As a consequence, the photopolymerization double bond conversions of MMA were not greatly increased as the concentrations of the photoinitiator **C3** or **C4** reached certain values [27].

Visible-light photopolymerization kinetics parameters of **S3** and **S4** measured by photo-DSC were summarized in **Table 2**. The data showed that the maximal percent of double bond conversion and the maximal photopolymerization rate of **S4** system were higher than those of **S3** respectively at the same conditions (such as at 0.3 mol%, **S4**,  $R_{p_{max}} (s^{-1})$ , 0.188, C%, 63.7%, **S3**;  $R_{p_{max}} (s^{-1})$ , 0.122, C%, 48.1%). It demonstrated that **C4** produced more effective visible light photoinitiating effect than **C3**. This could be mainly due to the presence of the cooperative photoinduced intramolecular electron transfer effect in **C4**.

We further compared the intramolecular photoinitiating polymerization effect of **S3** or **S4** to that of the corresponding intermolecular photosensitive initiating systems **S1** or **S2** under visible light irradiation. **Fig. 5** showed the variations of visible light photoinitiating polymerization efficiencies by **S1–S4** systems with the irradiation time at the same concentrations of photoinitiators and photosensitizers. The higher photoinitiating polymerization rate

and the smaller double bond conversion of MMA were obtained for **S3** and **S4** systems ( $R_{p_{max}} (s^{-1})$ , 0.0756, the final conversion 37.2% at 0.4 mol%) and **S2** system ( $R_{p_{max}} (s^{-1})$ , 0.113, the final conversion, 43.1%, at 0.4 mol%) comparing with **S3** ( $R_{p_{max}} (s^{-1})$ , 0.154, the final conversion 55.1% at 0.4 mol%) and **S4** ( $R_{p_{max}} (s^{-1})$ , 0.219, the final conversion 72.2% at 0.4 mol%) respectively. The results demonstrated that the active free radicals were produced by the intramolecular photoinduced electron transfer process in **S3** and **S4** systems more efficiently than the intermolecular photoinduced electron transfer process in **S1** and **S2** systems.

The visible light irradiation photoinitiating polymerization efficiency of MMA by **C3** or **C4** was also compared to that by titanocene. The results showed the **C3** and **C4** produced more visible light photoinitiating polymerization of MMA than titanocene at the same experimental conditions (the final conversion 44.2%,  $R_{p_{max}} (s^{-1})$ , 0.119, at 0.4 mol% of titanocene). This could be due to the larger visible absorption and the greater intramolecular electron transfer in **C3** and **C4** than those in titanocene. We also found that the other acrylate monomers such as 2-hydroxyethyl-methacrylate could be efficiently photoinitiated by **C4** under visible light irradiation (**Fig. S1**, Supplementary date, the final conversion 81.5%, at 0.4 mol%).

### 3.4. Molecular weight and polydispersity of photopolymer MMA

The photopolymers were yielded by **S1–S4** systems in ethyl acetate under visible light irradiation (wherein [MMA],  $1 \times 10^{-2}$  mol/L, the concentrations of the photoinitiators,  $2 \times 10^{-5}$  mol/L), which were precipitated in cold methanol, and washed by alcohol and dried in vacuum. We further determined the molecular weight and polydispersity of the above PMMAs according to the following equation:

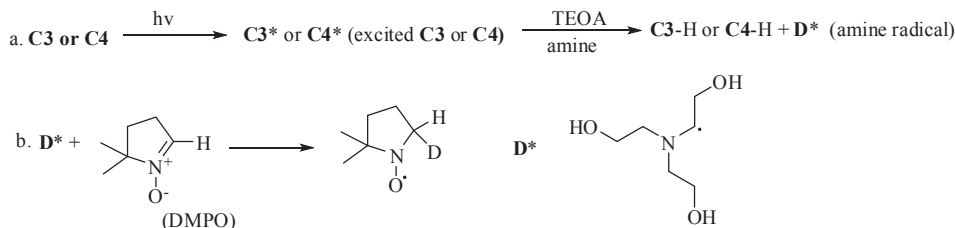
$$M_w/M_n = 1 + P \quad (3)$$

wherein  $P$  was the extent of the polymerization reaction. It is well-accepted that the lower value of  $P$  is, the greater the photoinitiating polymerization reaction extent is.

For the studied systems such as **S4**,  $P$  was 0.514 as the concentration of photoinitiator **C4** and coinitiator was  $1 \times 10^{-5}$  mol/L under 3 h of visible light irradiation ( $M_w$ ,  $7.216 \times 10^5$ ,  $M_n$ ,  $4.767 \times 10^5$ ). The other systems **S1**, **S2** and **S3** exhibited the larger  $P$  values at the same experimental conditions than **S4** (**S1**, 0.843, **S2**, 0.721, **S3**, 0.645), but these  $P$  values are lower than 1.00. The results showed that the yielded PMMA possessed not only a huge molecular weight, but a narrow polydispersity, suggesting that these systems underwent the fine visible light photoinitiating polymerization. In particular, **S4** produced the most excellent polydispersity of PMMA among the studied systems in this work.

### 3.5. Fluorescence quenching and laser flash photolysis

The fluorescence emission measurement showed that **C3** and **C4**



**Scheme 3.** The trapping mechanisms of free radical by DMPO.

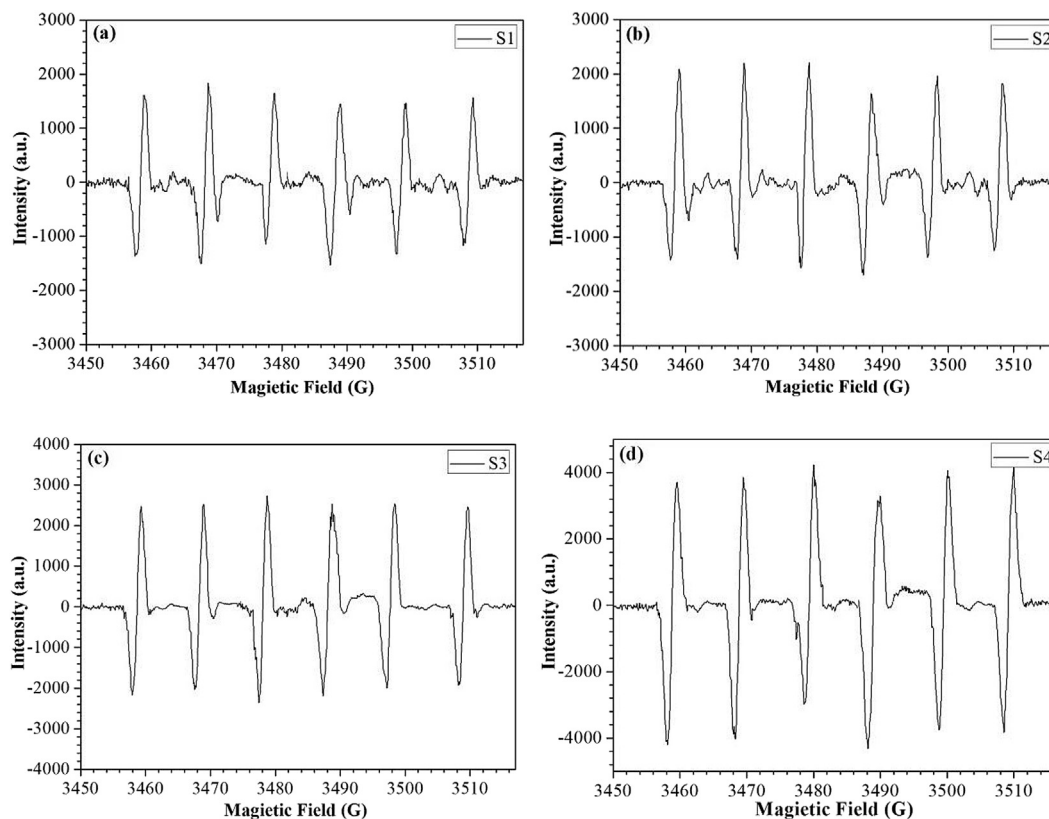


Fig. 9. The major ESR peaks of different photopolymerization systems in ethyl acetate, **S1**, 9(a) **S2**, 9(b) **S3**, 9(c) **S4**, 9(d).

possessed the small fluorescence quantum yields (such as in EtOAc, **C4**, 0.101), which increased the yields of the triplet states generating the initiating radicals. The fluorescence quenching studies of **C3** or **C4** by triethanolamine (coinitiator) were performed at the different concentrations, which was found to obey Stern–Volmer equation (i.e.,  $I_0/I = 1 + K_q \cdot \tau \cdot [Q]$ , Fig. 6). The quenching constants,  $K_q$ , obtained from the slopes were  $1.27 \times 10^{10} \text{ M}^{-1} \text{ s}^{-1}$  and  $1.93 \times 10^{10} \text{ M}^{-1} \text{ s}^{-1}$  for **C3** and **C4** respectively.

The laser flash photolysis experiments were carried out to investigate the properties of the triplet states of **C3** or **C4**. Fig. 7 showed the typical transient absorption spectra of **C3** after the irradiation of laser pulses at 355 nm. The yielded transient peak at around 530 nm was much similar to the triplet–triplet spectra of benzophenone, demonstrating that benzophenone segment increased the yield of the triplet state of the entire molecules. In addition, it was found that the transients could be efficiently quenched by oxygen, which further suggested that the transient peaks was assigned to triplet–triplet absorption. The further study showed that triethanolamine also could quench the transients, and the rate constants  $k_r$  were found as  $2.36 \times 10^9 \text{ M}^{-1} \text{ s}^{-1}$  and  $3.43 \times 10^9 \text{ M}^{-1} \text{ s}^{-1}$  for **C3** and **C4** respectively (Fig. 8).

### 3.6. ESR spectral analysis

The determination of ESR spectra was performed to get the information on visible photoinitiation mechanisms of **S1–S4** systems. The active free radicals with the short lifetime formed upon the irradiation were trapped by DMPO in spin-trapping experiments. The trapping mechanism of the radicals of **C3** or **C4** by DMPO was presented in Scheme 3.

The major ESR peaks shown in Fig. 9 suggested the presence of the same type of radicals produced by **S1–S4**, indicating that the

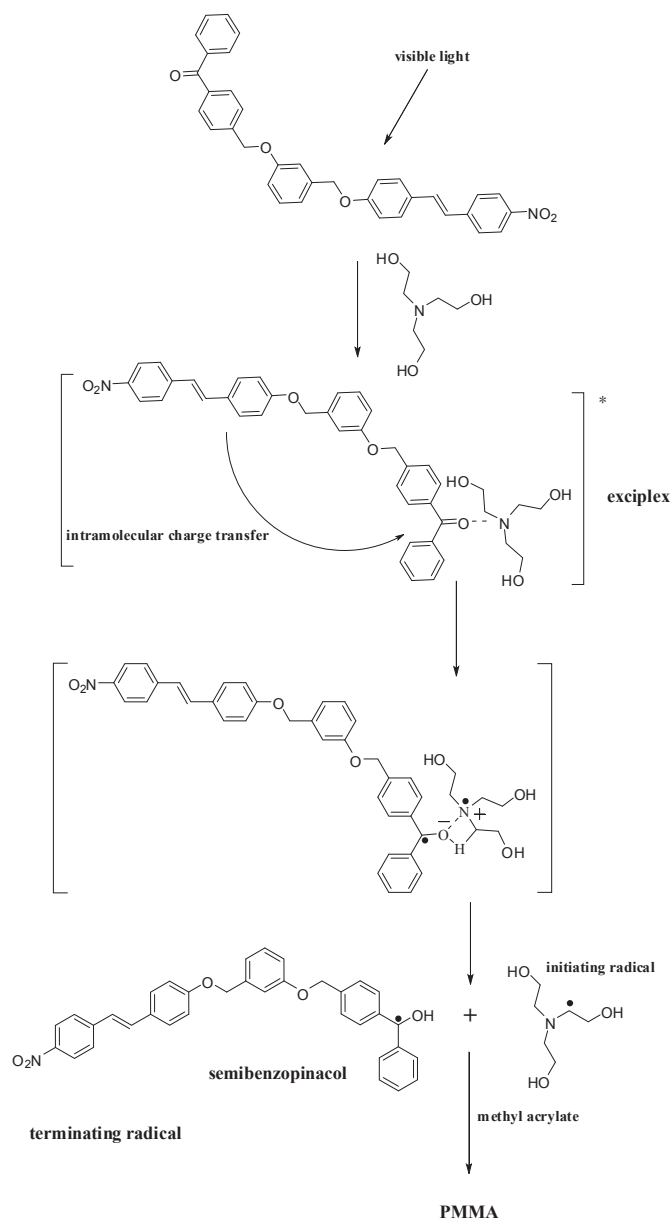
generating mechanism of the active free radicals by these systems could be similar. It was found that ESR spectra of **S1–S4** were quite similar to those of benzophenone–amine photoinitiators [28]. It was considered that under the incident visible light, the benzophenone part in **C3** or **C4** or benzophenone derivatives **C1** or **C2** could easily react with the coinitiator triethanolamine acting as the hydrogen donor to yield the active free radicals for the photoinitiating polymerization of acrylate monomers.

In addition, ESR signal intensities of the free active radicals of **S3** and **S4** were stronger than those of **S1** and **S2** respectively. In particular, **S4** exhibited the stronger signals of the free active radicals than **S3** under the same experimental conditions. The results explained why **C4** could visible light photoinitiate polymerization of MMA more effectively than **C3**.

It is found that there is absence of any overlap between the UV/visible absorption of **C1** and the fluorescence emission of **C5** (Fig. S2, supplementary date). This suggests that it is impossible to undergo photoinduced energy transfer from **C5** to **C1** under visible light irradiation. Although nitro is an electron-withdrawing group, the entire molecule **C5** *p*-methoxy-*p*'-nitro-stilbene could be used as an electron donor as it is excited by visible light.

In **S1** and **S2**, it was proposed the photoinduced intermolecular electron transfer occurred from the photosensitizer **C5** to UV photoinitiators **C1** and **C2** under visible light irradiation, which produced the negatively charged benzophenone derivatives. Hence, the rapid hydrogen abstracting from the coinitiator triethanolamine occurred, and the active free radicals were produced.

While for **S3** or **S4**, the proposed visible light photoinitiating mechanism was typically shown in Scheme 4. It was thought that the photoinduced intramolecular electron transfer occurred from the chromophore parts to benzophenone part in **C3** or **C4** under visible light irradiation. The photoinduced yielded negatively



**Scheme 4.** A proposed photoinitiating polymerization of MMA by **S3** system.

charged transferred species could form an exciplex with the co-initiator triethanolamine, and the active  $\alpha$ -aminoalkyl free radicals were produced through a four-cycle ring intermediate by abstracting proton from triethanolamine [29].

### 3.7. Photobleaching studies

Photobleaching of the visible light photoinitiating systems **S1–S4** was observed in ethyl acetate, suggesting the photoinduced decomposition of photosensitizers and photoinitiators caused by photoinduced inter or intra molecular electron transfer. The representative variations of UV/visible spectra of **S3** systems were shown in Fig. 10. It showed that the absorption of **C3** decreased with the increase of visible light irradiation time, suggesting that the photobleaching occurred.

Photobleaching ratios of **S1–S4** could be calculated by the following equation:

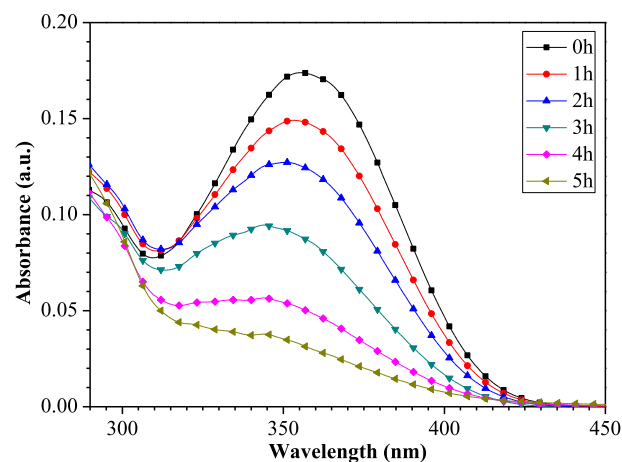


**Fig. 10.** The variations of UV/visible absorption spectra of **S3** system under different visible light irradiation time.

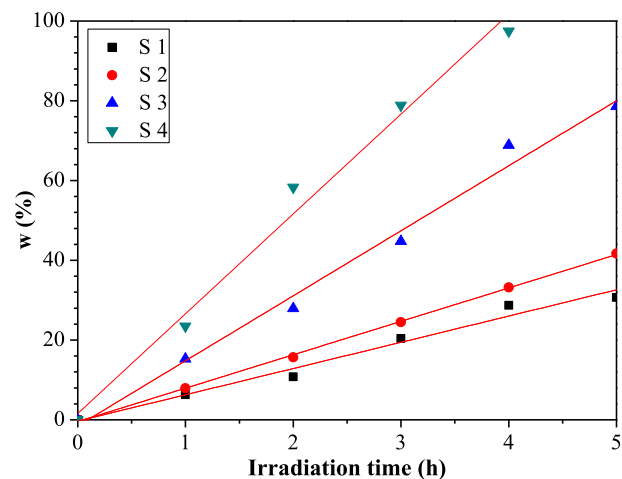


**Fig. 11.** The variations of photobleaching ratios of the systems at 360 nm under various visible light irradiation time.

$$w\% = \Delta A/A_0 = (A_0 - A_t)/A_0 \quad (4)$$

wherein  $A_0$  showed the optical density at the maximal absorption wavelength before the light irradiation, and  $A_t$  represented the absorption at 360 nm after time ( $t$ ) visible light irradiation.

Fig. 11 showed the plots of the decrease of the optical density at the maximal absorption wavelength of **S1–S4** with the irradiation time. The results suggested that **S4** yielded a greater photobleaching than **S3**, which further demonstrated that **S4** underwent more efficiently photochemical reaction than **S3**. This is mainly due to the presence of two benzophenone parts in **C4**, and thus the photoinduced intramolecular electron transfer is more efficient in **C4** than that in **C3**. As a consequence, **C4** produced the greater visible light photoinitiating polymerization of MMA than **C3**.

**Table 3**  
The estimated values of free energy change  $\Delta G$  between **C5** and **C1** or **C2**.

Compounds	$E_{RE(A)}$ (eV)	$E_{0,0}$ (eV)	$\Delta G$ (KJ/mol)
<b>C1</b>	−1.181	4.825	−444.9 KJ/mol
<b>C2</b>	−1.229	4.841	−449.5 KJ/mol

$E_{OX(D/D^+)} = -1.379$  eV for **C5**,  $E_{0,0} = hc/\lambda$ . 1 eV/atom = 96.15 KJ/mol, estimation from the fluorescence emission.

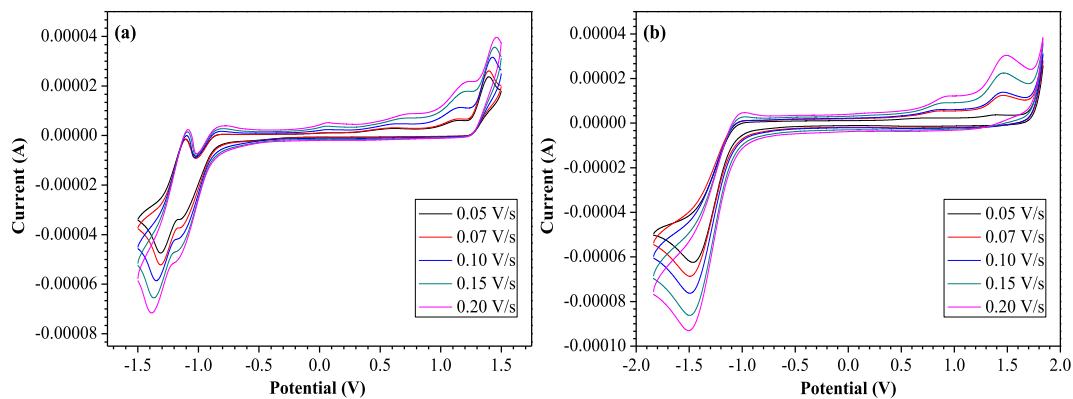


Fig. 12. The cyclic voltammograms of the new photoinitiators **C3** and **C4** in  $\text{CH}_2\text{Cl}_2$  at different scan rates.

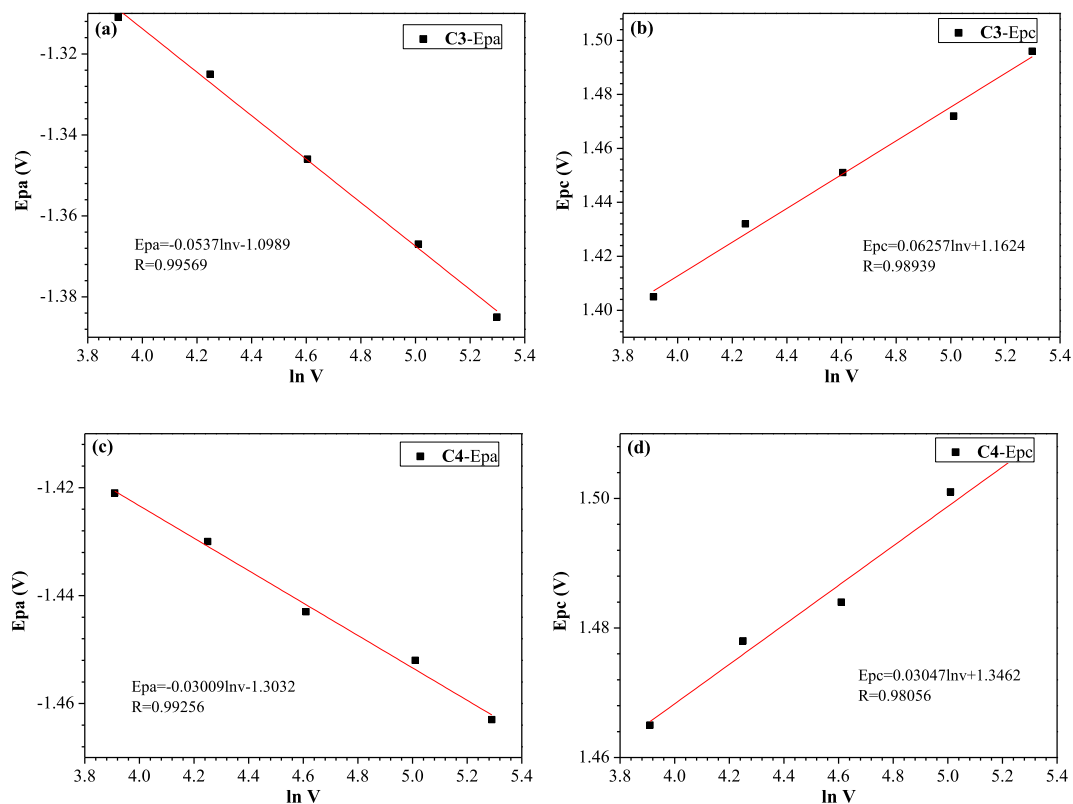


Fig. 13. The relationship between  $E_{pa}/E_{pc}$  and  $\ln v$  of **C3** and **C4** in methylene chloride.

In addition, Fig. 11 showed that **S3** and **S4** displayed the more effective photobleaching than **S1** and **S2** under visible light irradiation, which further demonstrated that the intramolecular photo-initiating system showed the more efficient photoinduced electron transfer than the corresponding intermolecular photosensitive initiating system. The results accounted for the more efficient visible light photoinitiating polymerization of MMA by **S3** or **S4** comparing to that by **S1** or **S2** correspondingly.

### 3.8. Cyclic voltammograms

We further measured the cyclic voltammograms of the target molecules to check the possibility of electron transfer. The value of free energy change  $\Delta G$  for the electron transfer reaction was estimated according to Rehm–Weller equation [30]:

$$\Delta G_{PET} = E_{OX(D/D^+)} - E_{RE(A)} - E_{0,0} \quad (5)$$

Where in  $E_{OX(D/D^+)}$  meant the potential of electron donors and  $E_{RE(A)}$  represented the potential of the acceptor,  $E_{0,0}$  was the excited state energy. In this study, **C1** or **C2** was used as the electron acceptors, while **C5** acted as the electron donor.

A large negative  $\Delta G$  shown in Table 3 suggested that photoinduced electron transfer between **C1** or **C2** and **C5** possessed a large thermos-driving force, and it was a spontaneous process. Thus, the results demonstrated that the intermolecular electron transfer between the photosensitizer **C5** and the UV photoinitiator **C1** or **C2** was allowed thermodynamically. As a result, it could be deduced that **C3** and **C4** could undergo intramolecular electron transfer between the dye part and benzophenone part through the linking covalent bond.

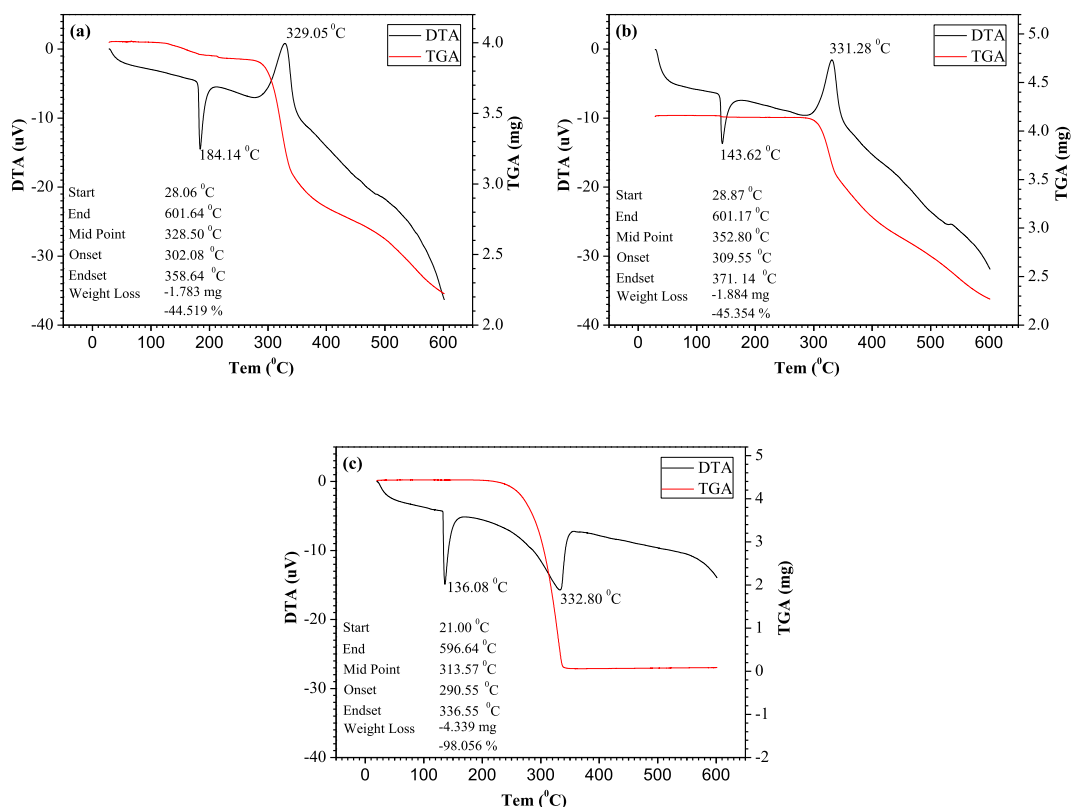


Fig. 14. DTA and TGA curves of **C3** (a), **C4** (b) and **C5** (c).

Fig. 12 showed the typical cyclic voltammograms of **C3** and **C4** in dichloromethane at various scan rates 0.05–0.20 V/s (Left/**C3**). One oxidation peak at  $-1.346$  V and one reduction peak at  $1.451$  V were observed at  $0.1$  V/s for **C3** (Left/ Fig. 12). Only one oxidation peak of **C4** was observed at  $-1.215$  V, and the reduction peak at  $1.193$  V could be regarded as the corresponding redox pair peak (Right/ Fig. 12).

Fig. 12 further suggested that with the increase of the scan rates, the anodic to cathodic peak current differed much from the unity and  $i_{pa}$  was not equaled to  $i_{pc}$ . It indicated the redox processes of **C3** and **C4** was completely irreversible under all the sweeping rates. In addition, it was also found that the redox process of **C3** and **C4** were dominated by the diffusion-controlled electron transfer reactions resulting from a linear increasing of the peak potentials with the square roots of the scan rates.

We calculated the internal electron transfer number of **C3** and **C4** based on cyclic voltammograms. The relationship between the peak potentials ( $E_{pa}$  and  $E_{pc}$ ) and the nature logarithm of the sweeping rate ( $\ln v$ ) was given in Fig. 13. The peak potentials were proportionally varied to  $\ln v$  with a linear regression equation. According to Laviron equation [31], the intramolecular electron transfer number could be calculated:

$$E_p = E^0 + (1 - \ln \nu)RT/\alpha nF \quad (6)$$

where in  $\alpha$  was the cathodic electron transfer coefficient (irreversible process  $\alpha=0.5$ ),  $n$  showed the electron transfer number.  $R$  represented the gas constant ( $R, 8.314 \text{ J}\cdot\text{mol}^{-1}\cdot\text{K}^{-1}$ ),  $T$  was the temperature in Kelvin ( $T = 298\text{K}$ ) and  $F$  meant the Faraday constant ( $F, 96493 \text{ C}\cdot\text{mol}^{-1}$ ). Hence, it was calculated  $n_{pa} = 0.95$ ,  $n_{pc} = 0.8$  for **C3**, and  $n_{pa} = 1.68$ ,  $n_{pc} = 1.70$  for **C4**. The results demonstrated that **C4** exhibited a greater internal electron transfer ability than **C3**. This could be ascribed to double intramolecular electron channels due to the presence of two benzophenone parts in **C4**.

### 3.9. Thermal stable analysis

The thermal properties of **C3** and **C4** were analyzed by the measurement of differential thermal analysis (DTA) and thermal gravity analysis (TGA) under  $\text{N}_2$  atmosphere. **C3**, **C4** and **C5** showed the different thermal decomposition temperatures. As shown in Fig. 14, the onset decomposition temperatures of **C3** and **C4** determined by TGA were  $302.08$  °C and  $309.55$  °C respectively, while the onset decomposition temperature of **C5** was  $290.81$  °C. The results suggested that the benzophenone part increased the thermal stability of the new photoinitiators.

In addition, **C3** and **C4** displayed the exothermic peaks at near  $330$  °C. At the endset temperature, the weight loss of **C3** was  $44.519\%$  at  $358.64$  °C, and the weight loss of **C4** was  $45.354\%$  at  $371.14$  °C, while **C5** showed an endothermic peak at  $336.55$  °C with  $98.056\%$  loss. In contrast, more than half of the weights of **C3** and **C4** were retained, and so they could be regarded as the robust molecules. The loss of weights of **C3** and **C4** could be caused by breaking the ether bonds. While in contrast, **C5** was nearly fully decomposed at the endset temperature. Furthermore, the endset temperature of the dyes followed the order **C4**>**C3**>**C5**. This meant that the thermal stabilities of new visible light photoinitiators **C3** and **C4** were increased by introducing benzophenone moiety.

## 4. Conclusions

In this study, the novel AB and AB<sub>2</sub> stilbene-benzophenone dyads were prepared for visible light photoinitiating polymerization of MMA studied by photo-DSC. The results demonstrated that **C4** yielded the greater visible light photoinitiating polymerization of MMA than **C3**. Furthermore, the dyads displayed the more efficient visible light photoinitiating polymerization of monomer

MMA comparing to the corresponding photoinduced intermolecular electron transfer systems. Laser flash photolysis provided the solid evidence of the triplet–triplet absorption of the dyads. The free radicals produced by the excited dyads were confirmed by ESR spectra. The large negative value of free energy change  $\Delta G$  suggested the presence of internal electron transfer in the new dyads. The cyclic voltammograms demonstrated that **C4** could undergo more intramolecular electron transfer than **C3**. In addition, the new dyads are thermal robust molecules. Hence, they could be used as the efficient visible light photoinitiators of acrylate monomers in various fields. The results shown in this work would be much beneficial for the preparation of new long wavelength thermal stable photoinitiators as required.

### Acknowledgments

We greatly thank the financial support from Natural Science Foundation of Chongqing (Nos. CSTC2012jjB50007 and CSTC2010BB0216). H. Li is grateful to the China Postdoctoral Science Foundation for the warm supporting to this work (Nos. 22012T50762 and 2011M501388).

### Appendix A. Supplementary data

Supplementary data related to this article can be found at <http://dx.doi.org/10.1016/j.dyepig.2016.04.035>.

### References

- [1] Buchalla W, Attin T. External bleaching therapy with activation by heat, light or laser—a systematic review. *Dent Mater* 2007;23:586–96.
- [2] Alexiades-Armenakas MR, Dover JS, Arndt KA. The spectrum of laser skin resurfacing: nonablative, fractional, and ablative laser resurfacing. *J Am Acad Dermatol* 2008;58:719–37.
- [3] Park YJ, Chae KH, Rawls HR. Development of a new photoinitiation system for dental light-cure composite resins. *Dent Mater* 1999;15:120–7.
- [4] Burget D, Mallein C, Fouassier JP. Photopolymerization of thiol–allyl ether and thiol–acrylate coatings with visible light photosensitive systems. *Polymer* 2004;45:6561–7.
- [5] Yang S, Megens M, Aizenberg J, Wiltzius P, Chaikin PM, Russel WB. Creating periodic three-dimensional structures by multibeam interference of visible laser. *Chem Mater* 2002;14:2831–3.
- [6] Yilmaz G, Tuzun A, Yagci Y. Thioxanthone–carbazole as a visible light photoinitiator for free radical polymerization. *J Polymer Sci Part A Polymer Chem* 2010;48:5120–5.
- [7] Paczkowski J, Kucybala Z. Generalization of the kinetic scheme for a dye-photosensitized free-radical polymerization initiating system via an intermolecular electron-transfer process. Application of Marcus theory. *Macromolecules* 1995;28:269–73.
- [8] Kabatc J, Pietrzak M, Paczkowski J. Cyanine borates revisited. Study of the kinetics of photoinitiated free radical polymerization via intermolecular electron transfer process. *J Chem Soc Perkin Trans* 2002;2(2):287–95.
- [9] Xiao P, Dumur F, Bui TT, Goubard F, Graff B, Morlet-Savary F, et al. Panchromatic photopolymerizable cationic films using indoline and squaraine dye based photoinitiating systems. *ACS Mac Lett* 2013;2(8):736–40.
- [10] He Y, Zhou W, Wu F, Li M, Wang E. Photoreaction and photopolymerization studies on squaraine dyes/iodonium salts combination. *J Photoch Photobio A Chem* 2004;162:463–71.
- [11] Chatterjee S, Gottschalk P, Davis PD, Schuster GB. Electron-transfer reactions in cyanine borate ion pairs: photopolymerization initiators sensitive to visible light. *J Am Chem Soc* 1988;110:2326–8.
- [12] Crivello JV, Bulut U. Curcumin: a naturally occurring long-wavelength photosensitizer for diaryliodonium salts. *J Polymer Sci Part A Polymer Chem* 2005;43:5217–31.
- [13] Kabatc J, Czech Z, Kowalczyk A. The application of halomethyl 1, 3, 5-triazine as a photoinitiator or co-initiator for acrylate monomer polymerization. *J Photoch Photobio A Chem* 2011;219:16–25.
- [14] Arioscia JA, Stansbury JW, Bowman CN. Evaluation and control of thiol–ene/thiol–epoxy hybrid networks. *Polymer* 2007;48:1526–32.
- [15] Hong KH, Liu N, Sun G. UV-induced graft polymerization of acrylamide on cellulose by using immobilized benzophenone as a photo-initiator. *Eur Polym J* 2009;45:2443–9.
- [16] Kawamura K, Kato K. Synthesis and evaluation as a visible-light polymerization photoinitiator of a new dye-linked bis (trichloromethyl)-1, 3, 5-triazine. *Polym Advan Technol* 2004;15:324–8.
- [17] Kawamura K. Novel and efficient dye-linked radical generators for visible light photoinitiating polymerization. *J Photochem Photobio A Chem* 2004;162:329–38.
- [18] Kawamura K, Yoshimasa A, Hideo T. Photoinduced intramolecular electron transfer between carbazole and bis (trichloromethyl)-s-triazine generating radicals. *J Phys Chem B* 2003;107:4579–86.
- [19] Gao F, Xu JQ, Yang YY, Li LD, Feng SJ. Visible light photopolymerization of methylmethacrylate initiated by titanocene. *J Photopolym Sci Tec* 1998;11(1):101–4.
- [20] Perrin D, Armarego W. Purification of laboratory chemicals. New York: Pergamon; 1996.
- [21] Eaton DF. Reference materials for fluorescence measurement. *Pure Appl Chem* 1988;60:1107–14.
- [22] Jiang X, Luo X, Yin J. Polymeric photoinitiators containing in-chain benzophenone and coinitiators amine: effect of the structure of coinitiator amine on photopolymerization. *J Photochem Photobio A Chem* 2005;174:165–70.
- [23] Itoh T, Hall Jr HK. 7-Chloro-7-phenyl-8, 8-dicyanoquinodimethane. A novel initiator for cationic polymerizations. *Macromolecules* 1990;23:4879–81.
- [24] Gao F, Hu N, Xie T, Cheng Z, Yang L, Liu X, et al. Study of the absorption and emission spectroscopy of “A–B” type photosensitive compounds including two-photon chromophore and benzophenone moiety. *Spectrochim Acta A* 2008;70:1006–12.
- [25] Grabowski ZR, Rotkiewicz K, Rettig W. Structural changes accompanying intramolecular electron transfer: focus on twisted intramolecular charge-transfer states and structures. *Chem Rev* 2003;103:3899–4032.
- [26] Lecamp L, Houllier F, Youssef B, Bunel C. Photoinitiated cross-linking of a thiol–methacrylate system. *Polymer* 2001;42:2727–36.
- [27] Zhou W, Liu Y, Bai L, Zhao N, Liu Y. Graft copolymerization of styrene onto casein initiated by potassium diperiodatonickelate (IV) in alkaline medium. *J App Polym Sci* 2006;100:4247–51.
- [28] Wei J, Wang H, Jiang X, Yin J. Novel photosensitive thio-containing polyurethane as macrophotoinitiator comprising side-chain benzophenone and co-initiator amine for photopolymerization. *Macromolecules* 2007;40:2344–51.
- [29] LaFratta CN, Fourkas JT, Baldacchini T, Farrer RA. Multiphoton fabrication. *Angew Chem Int Ed* 2007;46:6238–58.
- [30] Caronna T, Morrocchi S, Vittimberga BM. Importance of acidity on the energetically unfavorable electron-transfer reaction. An extension of the Rehm-Weller equation. Photoreaction of triplet 2, 4-pyridinedicarbonitrile with 2-propanol. *J Am Chem Soc* 1986;108:2205–8.
- [31] Luo H, Shi Z, Li N, Gu Z, Zhuang Q. Investigation of the electrochemical and electrocatalytic behavior of single-wall carbon nanotube film on a glassy carbon electrode. *Anal Chem* 2001;73:915–20.